Cellulose (2017) 24:4205–4216
DOI 10.1007/s10570-017-1430-7

ORIGINAL PAPER

Effect of fiber drying on properties of lignin containing cellulose nanocrystals and nanofibrils produced through maleic acid hydrolysis

Huiyang Bian · Liheng Chen · Hongqi Dai · J. Y. Zhu

Received: 28 April 2017 / Accepted: 27 July 2017 / Published online: 31 July 2017

Abstract The effect of fiber drying on the properties of lignin containing cellulose nanocrystals (LCNC) and nanofibrils (LCNF) produced using concentrated maleic acid hydrolysis of a never dried unbleached mixed hardwood kraft pulp was evaluated. Two drying conditions, i.e., air drying and heat drying at 105 °C were employed. It was found that drying (both air and heat) enhanced acid hydrolysis to result in slightly improved LCNC yields and less entangled LCNF. This is perhaps due to the fact that drying modified the cellulose supermolecular structure to become more susceptible to acid hydrolysis and the enhanced hydrolysis severity at the fiber surface when using dried fibers. Drying substantially improved LCNC crystallinity and LCNF suspension viscoelastic behavior. The present study quantitatively elucidated the effect of pulp drying (either air or heat) on producing cellulose nanomaterials and has practical importance because commercial market pulp (heat dried) is most likely to be used commercially.

Keywords Lignin containing cellulose nanocrystals and nanofibrils · Fiber drying and hornification · Maleic acid hydrolysis · Cellulose depolymerization · Rheological properties

Introduction

Cellulose nanomaterials, such as cellulose nanocrystals (CNC) and cellulose nanofibrils (CNF) have attracted growing research interest in recent years due to their excellent biocompatibility and biodegradability for multi-functional utilizations (Eichhorn et al. 2010; Kelly et al. 2013; Zhu et al. 2016). Achieving low-cost, energy efficient, and environmentally sustainable and tailored production, however, is the key to commercial success.

Currently, cellulose nanomaterials are produced mostly using chemical pulps through a variety of chemical or enzymatic pretreatment methods (Beck-Candanedo et al. 2005; Chen et al. 2015, 2016; Leung et al. 2011; Pääkko et al. 2007; Saito et al. 2009; Wang et al. 2016; Yarbrough et al. 2017; Zhu et al. 2011). A few studies have been carried out on the effects of

Electronic supplementary material The online version of this article (doi:10.1007/s10570-017-1430-7) contains supplementary material, which is available to authorized users.

H. Bian · H. Dai
Jiangsu Co-Innovation Center of Efficient Processing and Utilization of Forest Resources, Nanjing Forestry University, Nanjing 210037, China

H. Bian · J. Y. Zhu (✉)
Forest Products Laboratory, U.S. Department of Agriculture, U.S. Forest Service, Madison, WI 53726, USA
e-mail: jzhu@fs.fed.us

L. Chen
Key Laboratory of Biomaterials of Guangdong Higher Education Institutes, Department of Biomedical Engineering, Jinan University, Guangzhou 510632, China

feeding cellulose sources, lignin content, and processing methods on the properties of resultant cellulose nanomaterials (Bian et al. 2017a; Jia et al. 2017; Qing et al. 2013; Rojo et al. 2015; Sacui et al. 2014; Spence et al. 2010). Limited attention, however, has been paid to the potential effects of fiber drying on the properties of resultant cellulose nanomaterials. It is known that drying can affect cellulose supermolecular structure and thereby enhance acid hydrolysis using concentrated sulfuric acid solutions (Kontturi and Vuorinen 2008). This is especially true using fibers dried at a high temperature of 110 °C (Kontturi and Vuorinen 2008). It is anticipated that early commercial production of cellulose nanomaterials will most likely use commercial market pulps (heat dried). Therefore, studying the effects of pulp drying on the production of cellulose nanomaterials has practical importance.

The objective of the present study is to evaluate two drying conditions, air and heat (at 105 °C) drying, on yield and physicochemical properties of cellulose nanomaterials produced from a never dried commercial unbleached hardwood pulp using a concentrated di-carboxylic acid hydrolysis. Concentrated maleic acid (a di-carboxylic acid with low solubility) hydrolysis was used for its advantages in easing acid recycling, esterification of cellulose to result in carboxylated CNC and CNF to facilitate dispersion in aqueous processing and further functionalization, as well as minimal loss of carbohydrates to sugars, and less corrosive to equipment to reduce capital cost (Bian et al. 2017a; Chen et al. 2016; Wang et al. 2017). The goal of the present study is to quantify the potential effects of pulp drying on production of cellulose nanomaterials.

Experimental

Materials

Anhydrous maleic acid was purchased from Sigma-Aldrich (St. Louis, MO). Never dried virgin unbleached mixed hardwood (mainly birch and maple) kraft pulp (UHP) in suspension was complimentarily provided by the International Paper Company (Loveland, OH). The pulp has a lignin content of 3.9%. Never dried (ND), air dried (AD), and heat dried (HD) at 105 °C UHP fibers were used to study the effect of drying on producing lignin containing CNC (LCNC) and CNF (LCNF). Air drying and heat drying were conducted at ambient of 23.8 °C and in an oven of 105 °C for 24 h, respectively. The moisture contents of the dried pulp samples were measured. The two dried pulp samples were soaked in deionized (DI) water overnight, then disintegrated for 10,000 revolutions at 312 rpm and 2% consistency at room temperature using a disintegrator (Model 73-06-01, TMI, Ronkonkoma, New York, USA). All pulp samples were screened to remove shives (unbroken fiber bundles) and stored in sealed plastic bags before use.

Maleic acid hydrolysis

The same experimental procedure described in our previous studies was employed to produce LCNC and LCNF as shown in Fig. 1 (Bian et al. 2017a, b; Wang et al. 2017). Three maleic acid solutions of concentrations of 81.9, 60.4 and 60.0 wt% were prepared to result in the same average concentration of 60 wt% when including water contained in the 10 g in oven dry (OD) weight of ND (moisture 72.8%), AD (moisture 6.4%), and HD (moisture 0%) UHP fibers, respectively. The acid solutions were heated to 120 °C in a 500 mL three-necked round-bottom flask using a hot liquid glycerol bath. ND, AD, and HD UHP fibers of 10 g (OD weight) each was fed continuously into their corresponding heated acid solutions to result in a liquor to pulp ratio of 10:1 (w/w). The fiber suspensions were constantly agitated using a mechanical mixer at 300 rpm during reactions of varied length of 60, 90 or 120 min. Each reaction was quenched at the end of the hydrolysis by adding 200 mL DI water. The suspension was repeatedly washed and centrifuged at 10,000 rpm for 10 min (Sorvall Superspeed RC2-B, 5.75 inches rotator, Ivan Sorvall, Inc., Norwalk, CT) to remove excessive maleic acid. An aliquot of supernatant was taken for analysis of dissolved sugar content. The precipitated water-insoluble solids (WIS) was dialyzed until the conductivity of the liquid reaches approximately 1–2 μS/cm and no longer changed. The supernatant became turbid, suggesting the presence of LCNC. LCNC was collected from the supernatant after centrifuging the dialyzed WIS suspension at 10,000 rpm for 10 min twice. LCNC yield was determined using a COD method as described previously (Wang et al. 2012).

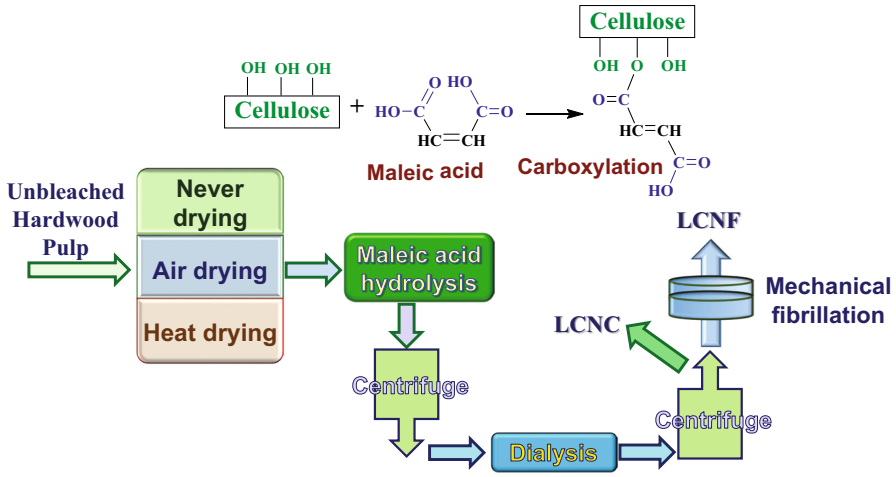

Fig. 1 A schematic experimental flow diagram for LCNC and LCNF production using concentrated maleic acid hydrolysis

LCNF production

The collected hydrolyzed lignocellulosic solid residue (LCSR) after separating LCNC from WIS was composed of partially hydrolyzed fibers (Fig. S1) that were used for producing LCNF through subsequent mechanical fibrillation using a microfluidizer (M-110EH, Microfluidics Corp., Westwood, MA) as demonstrated previously (Bian et al. 2017b; Wang et al. 2013). The LCSR slurry of approximately 1% consistency was fed through a 200 µm and an 87 µm chamber in series for either 1 or 5 passes at 100 MPa.

Chemical composition analyses

The chemical composition of the initial never dried UHP fibers and acid hydrolyzed WIS samples (Table S1) were analyzed by the Analytical Chemistry and Microscopy Laboratory (ACML) at the USDA Forest Service, Forest Products Laboratory, using an improved high-performance anion exchange chromatography with pulsed amperometric detection (HPAEC-PAD) method as described previously (Luo et al. 2010). All fiber samples were first digested using two-step sulfuric acid hydrolysis. The kappa number of the never dried pulp sample was measured according to TAPPI Standard Method T236 om-99 (TAPPI 1999).

Atomic force microscopy (AFM)

Suspensions of LCNC or LCNF approximately 0.01 wt% were deposited on a clean mica substrate and air-dried overnight in ambient for AFM (CS-3230, AFM workshop, Signal Hill, CA, USA) measurements as described previously (Bian et al. 2017b). Number averaged heights and lengths were measured using Gwyddion (Department of Nanometrology, Czech Metrology Institute, Crezh Republic, 64-bit) and Image-Pro Plus software (Media Cybernetics, Inc., Rockville, MD), respectively.

Degree of polymerization and X-ray diffraction analyses

Cellulose degree of polymerization (DP) was determined according to the TAPPI Standard Test Method T230 om-08 (TAPPI 2012) using 20 mL of cupriethylenediamine solution at 0.5 M to solubilize 0.10 g (OD) of fibrous solids. The lignin contained in the sample did not affect solubilization perhaps due to its low content of 3.9% (Kappa number of 23.2). The viscosity of the resultant solution was measured using a capillary viscometer (150 T447-T450, Cannon Instrument Company, State College, PA) at 25 °C. DP values were calculated as expressed by Eq. (1) (Mazumder et al. 2000).

$$DP^{0.905} = 0.75[954 \log X - 325] \quad (1)$$

where X is the viscosity of the resultant solution. Duplicate measurements were carried out and the averages were reported.

Wide angle X-ray diffraction (XRD) was used to measure crystallinity indices (CrI) of cellulosic samples on a Bruker D8 130 Discover system with Cu-Kα radiation (Bruker Corp., Billerica, MA, USA) at the

Material Science Center, University of Wisconsin, Madison, WI. CrI was calculated using Eq. (2) according to the Segal method (Segal et al. 1959) with or without background subtraction.

$$\mathrm{CrI} = \frac{I_{002} - I_{\mathrm{am}}}{I_{002}} \times 100\% \quad (2)$$

where I_{002} is the maximum peak intensity at a 2θ angle close to 22.5°, and I_{am} is the minimum diffraction intensity at a 2θ angle close to 18°.

Carboxyl content and surface charge

The carboxyl group content of LCNC and LCNF specimens was determined using conductometric titration as described previously (Bian et al. 2017a). LCNC (or LCNF) solution containing 50 mg LCNC (or LCNF) was mixed with 100 mL of 1 mM NaCl solution. Then the solution was titrated with 10 mM NaOH using a conductance meter (YSI Model 35, Yellow Springs Instrument Co., Ohio, USA). The amount of NaOH solution consumed to reach the lowest point of the titration curves was used to calculate carboxyl group content as follows:

$$C(\mathrm{mmol/g}) = \frac{c \times v}{m} \quad (3)$$

where C is the carboxyl group content (mmol/g), c is the concentration of NaOH solution (mmol/L), v is the volume of added NaOH solution (mL), m is the OD weight of the sample (g).

LCNC and LCNF surface charges were measured using a zeta potential analyzer (Nanobrook Omni, Brookhaven Instruments, Holtsville, NY) at ambient temperature using suspensions at approximately 0.5 g/L. Each sample was measured 5 cycles and the averages were presented.

Dynamic viscoelastic analyses

LCNF suspensions (ND-LCNF, AD-LCNF and HD-LCNF) at 1 wt% were transferred to airtight plastic bottles to minimize water evaporation. The rheological behaviors were analyzed with an Anton Paar MCR302 Rheometer (Anton Paar, Ashland, VA, USA) with a parallel plate geometry of 25 mm in diameter. The gap between the two plates was sealed using silicon oil with low viscosity. The dynamic strain sweep from 0.01 to 100% at $\omega = 10$ rad/s was first performed at 25 °C. The storage modulus was recorded to define the linear viscoelastic region (LVR) in which the storage modulus is independent of the strain amplitude. Dynamic frequency sweep was measured from 0.1 to 100 rad/s at 25 °C.

Fourier-transform infrared spectroscopy (FTIR)

FTIR analyses of the LCNC and LCNF samples along with the feed UHP fibers were carried out using a commercial FT-IR spectrophotometer (Spectrum 100, PerkinElmer, Waltham, MA) equipped with a universal attenuated-total-reflection (ATR) probe. All samples were freeze-dried before analyses.

Results and discussion

LCNC and LCNF yields

The yields of LCSR, LCNC along with glucose recovery from hydrolysate were listed in Table 1. To facilitate discussion, hydrolysis conditions were abbreviated as MxxTyyytzzz to represent maleic acid concentration xx% at temperature yyy in degree C for zzz min. LCNC yields were low with the highest yield of 6.6% obtained from AD-M60T120t180. Increasing acid concentration or temperature only increased LCNC yield slightly as can be seen from the yields of AD-M70T120t120 and AD-M60T130t120. Both types of drying resulted in a slight increase in LCNC yield under same hydrolysis conditions with the highest yield from the HD sample for each condition studied. An early study indicated that drying can alter the cellulose supermolecular structure to render cellulose more susceptible to acid hydrolysis (Kontturi and Vuorinen 2008). The observed drying effect on LCNC yield, perhaps, was also due to the enhanced local hydrolysis severity, because as-dried fibers were directly fed into the reactor, i.e., the actual acid concentration at fiber surface and in fiber pores during the early stage of hydrolysis was highest for the HD fibers followed by AD fibers. The water on the fiber surface and in the pores of ND fibers substantially diluted local acid concentration. It can take a long time to achieve local acid concentration equilibrium especially in the fiber pores where most reactions took place. An early study (Kontturi and Vuorinen 2008), however, found drying had no effect on CNC yield

Table 1 Yields of LCSR and LCNC, carboxyl group content, surface charge and crystallinity (CrI) of LCNC and LCNF (5 passes through the 200 and 87 μm chamber in the microfluidizer), and recovery of glucose from maleic acid hydrolysis of unbleached mixed hardwood pulp under different conditions

Sample label	LCNC yield (%)	LCSR yield (%)	Glucose recovery (%)	LCNC			LCNF		
				COOH (mmol/g)	Charge (mV)	CrI (%)	COOH (mmol/g)	Charge (mV)	CrI (%)
ND-M60T120t60	4.6	88.2	1.2	0.15	−24.5 ± 2.7	72.4	0.03	−22.8 ± 1.4	72.9
ND-M60T120t90	5.2	85.0	1.5	0.16	−29.7 ± 2.9	72.0	0.07	−25.6 ± 2.0	71.9
ND-M60T120t120	5.5	87.8	1.8	0.19	−34.1 ± 2.3	73.4	0.09	−29.1 ± 1.8	73.7
AD-M60T120t60	4.7	90.5	1.1	0.11	−29.7 ± 2.3	76.6	0.05	−25.4 ± 1.5	73.9
AD-M60T120t90	5.7	84.9	1.8	0.19	−37.9 ± 2.0	77.1	0.08	−30.4 ± 2.0	75.2
AD-M60T120t120	5.9	84.0	2.2	0.24	−49.1 ± 2.0	76.6	0.10	−41.7 ± 1.9	76.2
AD-M60T120t180	6.6	78.6	2.0	0.27	−43.7 ± 3.4	76.4	0.15	−38.7 ± 3.0	76.0
AD-M70T120t120	6.0	82.0	2.0	0.23	−48.2 ± 3.6	76.3	0.11	−49.2 ± 3.6	75.9
AD-M60T130t120	5.7	81.0	1.6	0.20	−45.4 ± 4.3	77.2	0.10	−36.1 ± 2.4	76.5
HD-M60T120t60	5.2	85.1	1.4	0.26	−42.3 ± 1.1	81.7	0.06	−33.6 ± 1.1	79.0
HD-M60T120t90	5.8	82.6	2.1	0.27	−45.6 ± 2.1	81.7	0.09	−38.6 ± 0.7	79.8
HD-M60T120t120	6.2	80.7	2.8	0.28	−49.3 ± 1.4	81.3	0.14	−42.9 ± 0.3	79.2

using concentrated sulfuric acid. The study was carried out by adding concentrated sulfuric acid solution in dropwise onto wet (ND) or rewetted (dried) pulp fibers. This procedure eliminated the enhanced local acid concentration effect observed in the present study. Furthermore, sulfuric acid is a very strong acid and CNC degradation to sugars is the dominant factor controlling CNC yield according to our previous studies (Chen et al. 2015; Wang et al. 2014) under the hydrolysis condition of 64 wt% at 45 °C for 25 min carried out by these authors. When using a weak acid such as maleic acid in the present study, hydrolysis of disordered cellulose is the dominant factor in controlling CNC yield (Chen et al. 2016). As a result, any increase in the extent of acid hydrolysis, either using more susceptible fibers through drying or enhanced local hydrolysis severity, can result in an improved CNC yield.

Dissolution of carbohydrates was low of approximately 20% or less as listed in Table 1. The remaining LCSR as partially hydrolyzed fibers was used to produce LCNF through subsequent mechanical fibrillation.

LCNC and LCNF morphologies

LCNC produced using maleic acid hydrolysis had relatively long length and thicker height compared with CNC samples produced using sulfuric acid (Chen et al. 2015), most likely due to the weaker acidity of maleic acid. The number averaged lengths and heights of LCNC were in the range of 200–450 nm and 10–30 nm, respectively, as shown in Fig. 2. LCNC length and height from both AD and HD fibers appeared to be shorter and narrower than the corresponding LCNC length and height from ND fibers. Furthermore, this shortening and narrowing effect is more pronounced for the HD-LCNC as can be clearly seen from the LCNC height distributions under the three hydrolysis conditions compared in Fig. 2. Careful examination of the AFM images found that more crystal bundles present in the LCNC sample produced using ND fibers than those from the AD and HD fibers (comparing Fig. 2a and b with d and e, or g and h, respectively). The observed drying effect on LCNC size is in agreement with an early study using sulfuric acid hydrolysis of bleached softwood kraft pulp (Kontturi and Vuorinen 2008). These authors attributed this effect to the change of cellulose supermolecular structure through drying to render the "amorphous" or disordered cellulose in a higher energy state. As a result, dried fibers are more susceptible to acid hydrolysis. A more efficient hydrolysis of disordered cellulose certainly reduced crystal length and width especially in the present study that used a weak acid of maleic acid. We believe that this phenomenon can also

be attributed to the enhanced local acid hydrolysis severity when using either AD or HD fibers as discussed in the previous section. Increasing acid hydrolysis severity through extended reaction time reduced the differences in LCNC size among ND, AD, and HD samples (comparing Fig. 2j with l, Fig. 2m with o). A longer reaction time, perhaps, reduced the effect of enhanced local acid concentration effect during hydrolyzing AD and HD fibers. Globular lignin particles were also observed in all LCNC samples which can affect LCNC hydrophobicity as we revealed previously (Bian et al. 2017a).

Subsequent mechanical fibrillation of LCSR with only one pass (low energy input) through the 200 and 87 μm chamber of the microfluidizer produced LCNF also with varied morphologies as shown in Fig. 3. Mechanical force reduced fibril length as evidenced by the measured cellulose degree of polymerization (DP) as listed in Table S2. LCNF contained large fiber bundles with lengths and heights ranging from 500 to 1000 nm and 6–30 nm as shown by AFM images (Fig. 3). Similar to LCNC, LCNF from ND sample also have thicker height than those from AD and HD ones as shown in Fig. 3j–l. Increasing the numbers of passes through the microfluidizer resulted in shorter and thinner fibrils (comparing Fig. 3 with S2).

Aspect ratio is an important parameter for cellulose nanomaterials. LCNC length was measured from the AFM images by randomly picking over 150 crystals. Similar practice was carried out for LCNF (Fig. S3), but with less accuracy due to entanglement (Fig. 3a–i), therefore DP was used as a measure of LCNF length. The AFM measured the heights of LCNC and LCNF were linearly correlated to LCNC length and LCNF DP as shown in Fig. 4a and b, respectively. This indicates that the mean LCNC or LCNF aspect ratio is not much affected by chemical and mechanical processing conditions, i.e., the mean aspect ratio, inverse of the slope, for the LCNC and LCNF produced in this study was approximately 11 and 16, respectively. Previously, we proposed a fiber longitudinal hierarchical structure model that hypothesize cellulose nanofibrils aggregate in the longitudinal direction to form microfibrils (Qin et al. 2016). This suggests that cellulose depolymerization is necessary to produce nanofibrils. Under a certain range of processing conditions, the mean aspect ratio of cellulose nanomaterials may not be affected by processing conditions. The slopes shown in Fig. 4a and b, however, vary substantially from those reported in the previous study (Qin et al. 2016) that used dilute oxalic acid hydrolysis of bleached eucalyptus pulp fibers to produce CNF through subsequent mechanical fibrillation in a stone disk grinder, indicating that fiber source and large variations in processing conditions can affect aspect ratio.

Fig. 2 AFM topographic images of LCNC produced from never dried (**a–c**, *top row*), air dried (**d–f**, *second row*) and heat dried (**g–i**, *third row*) pulp fibers at maleic acid concentration 60 wt% and 120 °C for 60 (*left panel*), 90 (*middle panel*), 120 (*right panel*) min. Scale = 1 μm. **a** ND-M60T120t60, mean height = 25.9 nm; **b** ND-M60T120t90, mean height =17.3 nm; **c** ND-M60T120t120, mean height = 14.5 nm; **d** AD-M60T120t60, mean height = 25.8 nm; **e** AD M60T120t90, mean height = 14.5 nm; **f** AD-M60T120t120, mean height = 10.8 nm; **g** HD-M60T120t60, mean height = 17.9 nm; **h** HD-M60T120t90, mean height = 12.6 nm; **i** HD-M60T120t120, mean height = 9.5 nm. (**j–l**) Comparisons of the AFM measured LCNC crystal height distributions. (**m–o**) Comparisons of the AFM measured LCNC length distributions

LCNC and LCNF crystallinities

The crystallinity indices (*CrI*) of the LCNC and LCNF samples were all higher than the *CrI* of the original unbleached pulp fibers of 71.4% (Tables 1 and S3). Except for ND-LCNC samples that have similar *CrI* to their corresponding LCNF, *CrI* of LCNC samples are slightly higher (0.4–2.7%) than their corresponding LCNF samples (71.9–79.8%, without baseline subtraction). Furthermore, *CrI* of LCNC (∼76%) or LCNF (75%) produced from AD fibers are approximately 1–5% higher than the *CrI* of their corresponding sample from ND fibers. *CrI* of LCNC and LCNF from HD fibers under the same processing conditions were the highest of approximately 81 and 79%, respectively. Because maleic acid is a weak acid, increasing local acid hydrolysis severity and the improved susceptibility of AD and HD fibers resulted in increased *CrI*. The X-ray diffraction spectra clearly shows the increased *CrI* of LCNC from AD and HD fibers (Fig. S4).

Carboxylation and surface charge

Conductometric titration of LCNC samples was conducted to quantify the carboxyl group content of the samples resulted from Fischer–Speier esterification by maleic acid (Fischer and Speier 1895). As

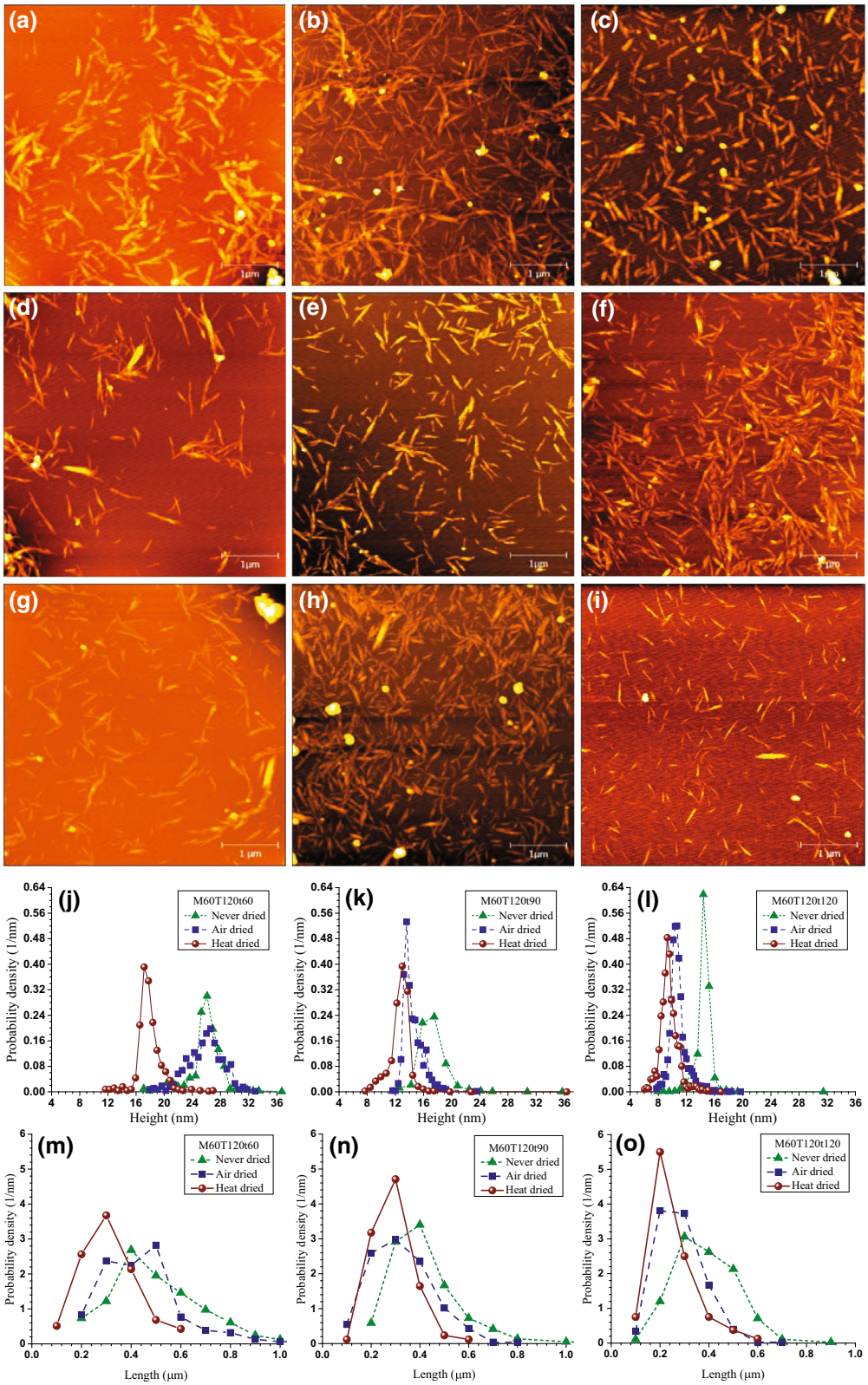
(a)
(b)
(c)
(d)
(e)
(f)
(g)
(h)
(i)
(j)
M60T120t60
Never dried
Air dried
Heat dried
Probability density (1/nm)
Height (nm)
(k)
M60T120t90
Never dried
Air dried
Heat dried
Probability density (1/nm)
Height (nm)
(l)
M60T120t120
Never dried
Air dried
Heat dried
Probability density (1/nm)
Height (nm)
(m)
M60T120t60
Never dried
Air dried
Heat dried
Probability density (1/nm)
Length (μm)
(n)
M60T120t90
Never dried
Air dried
Heat dried
Probability density (1/nm)
Length (μm)
(o)
M60T120t120
Never dried
Air dried
Heat dried
Probability density (1/nm)
Length (μm)

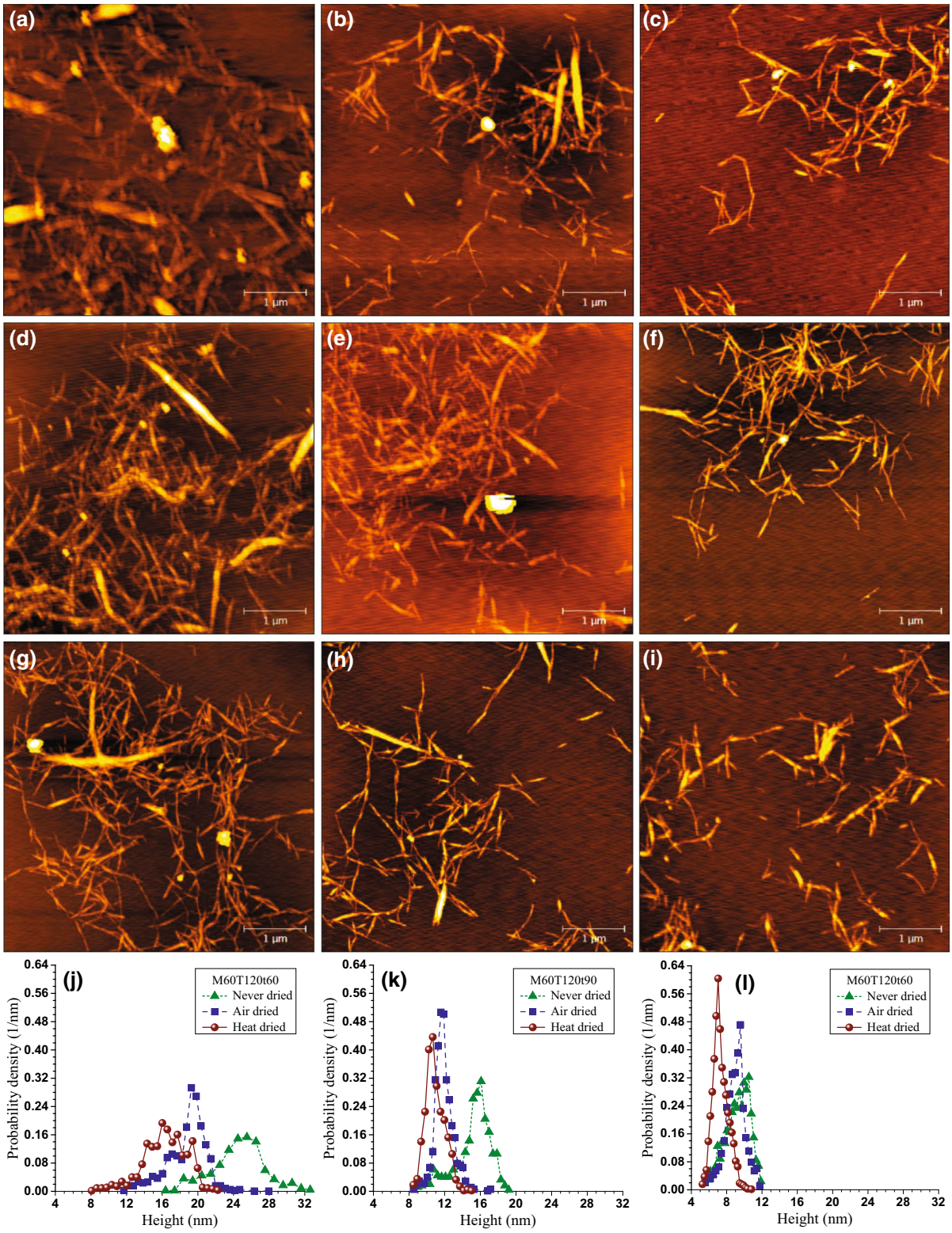
(a)
(b)
(c)
(d)
(e)
(f)
(g)
(h)
(i)
1 µm
(j)
M60T120t60
Never dried
Air dried
Heat dried
(k)
M60T120t90
Never dried
Air dried
Heat dried
(l)
M60T120t60
Never dried
Air dried
Heat dried
Probability density (1/nm)
Height (nm)
0.00
0.08
0.16
0.24
0.32
0.40
0.48
0.56
0.64
4
8
12
16
20
24
28
32

◀**Fig. 3** AFM topographic images of LCNF produced from LCSR after passing through 200 and 87 µm chamber for 1 pass at 100 MPa. Scale = 1 µm. LCSR were from using ND (*top row*), AD (*second row*), and HD (*third row*) at maleic acid concentration 60 wt% and 120 °C for 60 (*left panel*), 90 (*middle panel*), 120 (*right panel*) min. **a** ND-M60T120t60, mean height = 24.9 nm; **b** ND-M60T120t90, mean height = 15.2 nm; **c** ND-M60T120t120, mean height = 9.3 nm; **d** AD-M60T120t60, mean height = 18.7 nm; **e** AD-M60T120t90, mean height = 11.9 nm; **f** AD-M60T120t120, mean height = 9.0 nm; **g** HD-M60T120t60, mean height = 16.3 nm; **h** HD-M60T120t90, mean height = 10.9 nm; **i** HD-M60T120t120, mean height = 7.3 nm. **j–l** Comparisons of the AFM measured LCNF fibril height distributions

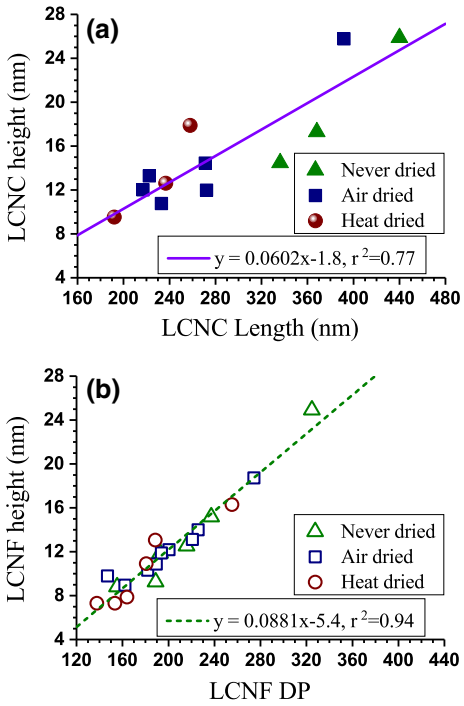

Fig. 4 Correlations between AFM measured mean LCNC heights with their mean lengths and LCNF heights with their mean degree of polymerization (DP) from all the experiments conducted

listed in Table 1, carboxyl group contents of LCNC samples ranged from 0.11 to 0.28 mmol/g. LCNF samples were less carboxylated compared with their corresponding LCNC with carboxyl groups less than 0.15 mmol/g. This is in agreement with our previous study (Bian et al. 2017a; Chen et al. 2016; Wang et al. 2017). In general, the data indicate that AD and HD fibers, especially HD fibers, resulted in enhanced carboxylation for both LCNC and LCNF. The data also show that increasing hydrolysis severity increased carboxylation to result in a good correlation between LCNC carboxyl group content and LCNC yield (Fig. S5). Surface carboxylation was also verified by Fourier transform infrared (FT-IR) analysis (Fig. S6). The most distinct spectral feature was the ester group of carboxylic acid at 1724 cm^{-1} as observed from LCNC and LCNF samples but not from the original fibers.

The surface carboxylation resulted in charged LCNC with good dispersion in water due to electrostatic repulsion. LCNC from HD fibers had highest zeta-potential under the same reaction conditions, suggesting using dried fibers was favorable for fiber esterification. This is a direct result of enhanced surface dehydration esterification when using dried fibers. LCNF samples had a non-detectable carboxyl groups with lower surface charge than LCNC, suggesting LCNC suspension was more stable than their corresponding LCNF suspension. Overall, the surface charges of LCNC and LCNF samples are proportional to their carboxyl group contents (Fig. S7).

Dynamic rheology analysis

The variations in LCNC and LCNF morphology and surface chemical properties will affect LCNC and LCNF suspension rheological properties (Fig. S8). Since such variations among LCNF samples are greater than among LCNC samples, the shear storage modulus G′ and loss storage modulus G″ of LCNF suspensions at 1 wt% consistency were compared. All LCNF colloidal suspensions show typical elastic response based on the results from dynamic strain sweep measurements shown in Fig. 5a. Within the LVR, these LCNF suspensions behaved like a viscoelastic solid with G′ values basically independent of the applied shear strain γ. Both G′ and G″ values gradually decreased with the continued increase in γ, indicating a transition of the LCNF samples from quasi-solid state to a quasi-liquor state. Based on these results, $\gamma = 0.1\%$ was chosen in the subsequent frequency sweep to ensure that dynamic oscillatory deformation of each suspension was within LVR. The corresponding maximum G′ (G_{max}') were 2243, 334 and 123 Pa (Fig. 5b) for ND-LCNF, AD-LCNF and HD-LCNF, respectively. As noted from Fig. 5a, LCNF from never dried fibers present the highest G_{max}', compared with those of the AD-LCNF and HD-

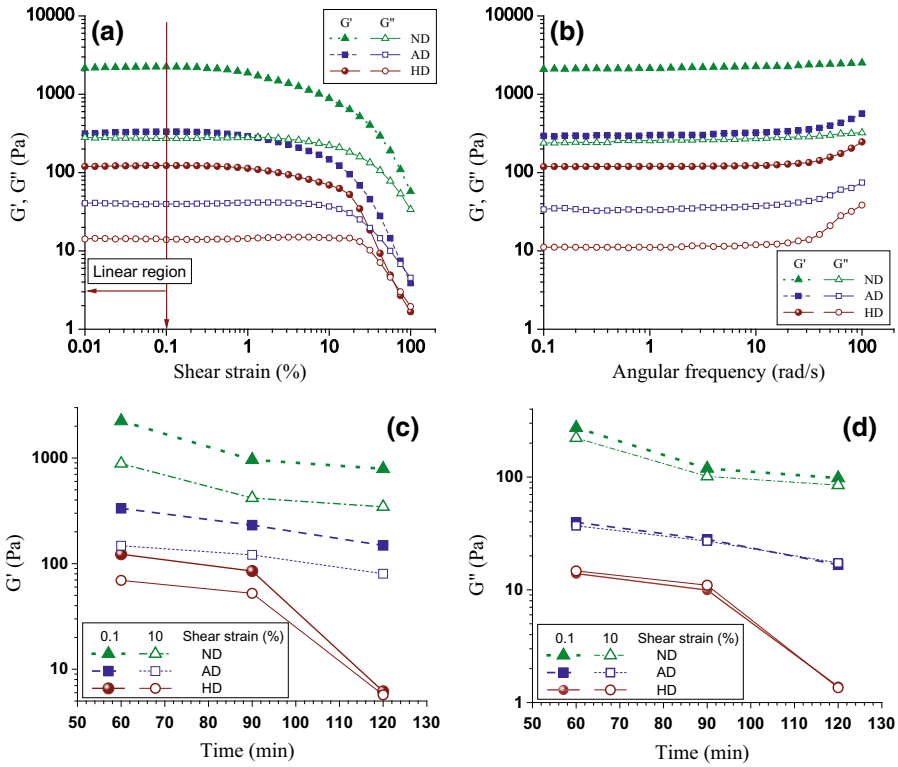

Fig. 5 Dynamic viscoelasticity behavior of LCNF colloidal suspensions of 1 wt% at 25 °C. LCNF were produced under M60T120t60 with one pass through 200 and 87 μm chamber in microfluidizer: **a** Strain dependence of shear storage modulus (G') and loss modulus (G''), measured at ω = 10 rad/s; **b** angular frequency (ω) dependence of G' and G'' measured at shear strain rate = 0.1%; **c** and **d** effect of hydrolysis severity (time) on G′ and G″, respectively

LCNF. This suggests that ND fibers, perhaps, were less susceptible to acid hydrolysis than AD and HD (Fig. S1) ones to result in LCNF with larger networks or longer and thick fibrils. This is supported by the AFM images shown in Fig. 3.

Increasing acid hydrolysis time increased hemicellulose dissolution and cellulose depolymerization (Table S2) to result in less entangled fibril network (Wang et al. 2017) and thinner fibrils (Fig. 3). This hydrolysis time effect on LCNF morphology affected the rheology of LCNF suspension as can be clearly seen from Fig. 5c and d. Both G′ and G″ decreased with hydrolysis time substantially at the shear strain rate of 0.1 and 10%.

Conclusions

This study quantified the effects of fiber drying on the properties of lignin containing nanocrystals (LCNC) and nanofibrils (LCNF) using never dried unbleached kraft mixed hardwood pulp through concentrated maleic acid hydrolysis. As a di-carboxylic acid with low solubility, maleic acid could be readily recovered using the mature crystallization technology. Maleic acid also esterified cellulose to result in carboxylated LCNC and LCNF. Both air and heat dried, especially heat dried, fibers were more susceptible to acid hydrolysis to result in more carboxylated, crystalline LCNC and LCNF with thinner crystals and less entangled fibrils. This is attributed to the enhanced local hydrolysis severity and susceptibility to hydrolysis of dried fibers. Fibril DP and crystal length and height measurements indicated that measured mean LCNC length or LCNF DP and their respective height were linearly correlated, suggesting processing conditions did not affect LCNF or LCNC mean aspect ratio within the conditions investigated, this validated the fiber longitudinal aggregation model proposed previously, furthermore cellulose deplymerization is necessary for cellulose nanomaterial production.

Acknowledgments This work was partially supported by US Forest Service, the Chinese State Forestry Administration (Project No. 2015-4-54), and the Doctorate Fellowship Foundation of Nanjing Forestry University. Funding from these programs made the visiting appointments of Bian at FPL possible. We also would like to acknowledge Dr. Goyal Gopal and his colleagues of International Paper Company for complimentarily providing us the unbleached mixed hardwood

pulp samples. Fred Matt of FPL conducted carbohydrate analyses and Carlos Baez conducted sample crystallinity analyses using XRD.

References

Beck-Candanedo S, Roman M, Gray DG (2005) Effect of reaction conditions on the properties and behavior of wood cellulose nanocrystal suspensions. Biomacromol 6:1048–1054

Bian H, Chen L, Dai H, Zhu JY (2017a) Integrated production of lignin containing cellulose nanocrystals (LCNC) and nanofibrils (LCNF) using an easily recyclable di-carboxylic acid. Carbohydr Polym 167:167–176

Bian H, Chen L, Wang R, Zhu JY (2017b) Green and low-cost production of thermally stable and carboxylated cellulose nanocrystals and nanofibrils using highly recyclable dicarboxylic acids. J Vis Exp. doi:10.3791/55079

Chen L, Wang Q, Hirth K, Baez C, Agarwal UP, Zhu JY (2015) Tailoring the yield and characteristics of wood cellulose nanocrystals (CNC) using concentrated acid hydrolysis. Cellulose 22:1753–1762

Chen L, Zhu JY, Baez C, Kitin P, Elder T (2016) Highly thermal-stable and functional cellulose nanocrystals and nanofibrils produced using fully recyclable organic acids. Green Chem 18:3835–3843

Eichhorn SJ, Dufresne A, Aranguren M, Marcovich NE, Capadona JR, Rowan SJ, Weder C, Thielemans W, Roman M, Renneckar S, Gindl W, Veigel S, Keckes J, Yano H, Abe K, Nogi M, Nakagaito AN, Mangalam A, Simonsen J, Benight AS, Bismarck A, Berglund LA, Peijs T (2010) Review: current international research into cellulose nanofibres and nanocomposites. J Mater Sci 45(1):1–33

Fischer E, Speier A (1895) Darstellung der Ester. Chem Ber 28(3):3252–3258

Jia C, Chen L, Shao Z, Agarwal UP, Hu L, Zhu JY (2017) Using a fully recyclable dicarboxylic acid for producing dispersible and thermally stable cellulose nanomaterials from different cellulosic sources. Cellulose 24(6):2483–2498

Kelly JA, Shukaliak AM, Cheung CCY, Shopsowitz KE, Hamad WY, MacLachlan MJ (2013) Responsive photonic hydrogels based on nanocrystalline cellulose. Angew Chem Int Ed 52(34):8912–8916

Kontturi E, Vuorinen T (2008) Indirect evidence of supramolecular changes within cellulose microfibrils of chemical pulp fibers upon drying. Cellulose 16(1):65–74

Leung ACW, Hrapovic S, Lam E, Liu Y, Male KB, Mahmoud KA, Luong JHT (2011) Characteristics and properties of carboxylated cellulose nanocrystals prepared from a novel one-step procedure. Small 7(3):302–305

Luo X, Gleisner R, Tian S, Negron J, Horn E, Pan XJ, Zhu JY (2010) Evaluation of mountain beetle infested lodgepole pine for cellulosic ethanol production by SPORL pretreatment. Ind Eng Chem Res 49(17):8258–8266

Mazumder BB, Ohtani Y, Cheng Z, Sameshima K (2000) Combination treatment of kenaf bast fiber for high viscosity pulp. J Wood Sci 46(5):364–370

Pääkko M, Ankerfors M, Kosonen H, Nykänen A, Ahola S, Österberg M, Ruokolainen J, Laine J, Larsson PT, Ikkala O, Lindström T (2007) Enzymatic hydrolysis combined with mechanical shearing and high-pressure homogenization for nanoscale cellulose fibrils and strong gels. Biomacromol 8:1934–1941

Qin Y, Qiu X, Zhu JY (2016) Understanding longitudinal wood fiber ultra-structure for producing cellulose nanofibrils using disk milling with dilute acid prehydrolysis. Sci Rep 6:35602

Qing Y, Sabo R, Zhu JY, Agarwal U, Cai Z, Wu Y (2013) A comparative study of cellulose nanofibrils disintegrated via multiple processing approaches. Carbohydr Polym 97(1):226–234

Rojo E, Peresin MS, Sampson WW, Hoeger IC, Vartiainen J, Laine J, Rojas OJ (2015) Comprehensive elucidation of the effect of residual lignin on the physical, barrier, mechanical, and surface properties of nanocellulose films. Green Chem 17:1853–1866

Sacui IA, Nieuwendaal RC, Burnett DJ, Stranick SJ, Jorfi M, Weder C, Foster EJ, Olsson RT, Gilman JW (2014) Comparison of the properties of cellulose nanocrystals and cellulose nanofibrils isolated from bacteria, tunicate, and wood processed using acid, enzymatic, mechanical, and oxidative methods. ACS Appl Mater Interfaces 6(9):6127–6138

Saito T, Hirota M, Tamura N, Kimura S, Fukuzumi H, Heux L, Isogai A (2009) Individualization of nano-sized plant cellulose fibrils by direct surface carboxylation using TEMPO catalyst under neutral conditions. Biomacromol 10(7):1992–1996

Segal L, Creely JJ, Martin AE, Conrad CM (1959) An empirical method for estimating the degree of crystallinity of native cellulose using the X-ray diffractometer. Text Res J 29:786–794

Spence KL, Venditti RA, Rojas OJ, Habibi Y, Pawlak JJ (2010) The effect of chemical composition on microfibrillar cellulose films from wood pulps: water interactions and physical properties for packaging applications. Cellulose 17(4):835–848

TAPPI (1999) TAPPI standard method (T236 om-99), Kappa number of pulp. Technical association of the pulp and paper industry. TAPPI Press, Atlanta, GA

TAPPI (2012) TAPPI standard test method (T230 om-08), viscosity of pulp (capillary viscometer method)

Wang QQ, Zhu JY, Reiner RS, Verrill SP, Baxa U, McNeil SE (2012) Approaching zero cellulose loss in cellulose nanocrystal (CNC) production: recovery and characterization of cellulosic solid residues (CSR) and CNC. Cellulose 19(6):2033–2047

Wang QQ, Zhu JY, Considine JM (2013) Strong and optically transparent films prepared using cellulosic solid residue (CSR) recovered from cellulose nanocrystals (CNC) production waste stream. ACS Appl Mater Interfaces 5(7):2527–2534

Wang Q, Zhao X, Zhu JY (2014) Kinetics of strong acid hydrolysis of a bleached kraft pulp for producing cellulose nanocrystals (CNCs). Ind Eng Chem Res 53(27):11007–11014

Wang W, Mozuch MD, Sabo RC, Kersten P, Zhu JY, Jin Y (2016) Endoglucanase post-milling treatment for producing cellulose nanofibers from bleached eucalyptus fibers by a supermasscolloider. Cellulose 23(3):1859–1870

Wang R, Chen L, Zhu JY, Yang R (2017) Tailored and integrated production of carboxylated cellulose nanocrystals

(CNC) with nanofibrils (CNF) through maleic acid hydrolysis. ChemNanoMat 3(5):328–335

Yarbrough JM, Zhang R, Mittal A, Vander Wall T, Bomble YJ, Decker SR, Himmel ME, Ciesielski PN (2017) Multifunctional cellulolytic enzymes outperform processive fungal cellulases for coproduction of nanocellulose and biofuels. ACS Nano 11(3):3101–3109

Zhu JY, Sabo R, Luo X (2011) Integrated production of nanofibrillated cellulose and cellulosic biofuel (ethanol) by enzymatic fractionation of wood fibers. Green Chem 13(5):1339–1344

Zhu H, Luo W, Ciesielski PN, Fang Z, Zhu JY, Henriksson G, Himmel ME, Hu L (2016) Wood-derived materials for green electronics, biological devices, and energy applications. Chem Rev 116(16):9305–9374